AJNR

Predicting Post-Operative Side Effects in VIM MRgFUS based on THalamus Optimized Multi Atlas Segmentation (THOMAS) on white-matter-nulled MRI: A Retrospective Study

Sonoko Oshima, Asher Kim, Xiaonan R. Sun, Ziad Rifi, Katy A. Cross, Katherine A. Fu, Noriko Salamon, Benjamin M. Ellingson, Ausaf A. Bari and Jingwen Yao

AJNR Am J Neuroradiol published online 9 August 2024
http://www.ajnr.org/content/early/2024/08/09/ajnr.A8448

Published August 9, 2024 as 10.3174/ajnr.A8448

ORIGINAL RESEARCH

Predicting Post-Operative Side Effects in VIM MRgFUS based on THalamus Optimized Multi Atlas Segmentation (THOMAS) on white-matter-nulled MRI: A Retrospective Study

Sonoko Oshima, Asher Kim, Xiaonan R. Sun, Ziad Rifi, Katy A. Cross, Katherine A. Fu, Noriko Salamon, Benjamin M. Ellingson, Ausaf A. Bari, Jingwen Yao

ABSTRACT

BACKGROUND AND PURPOSE: Precise and individualized targeting of the ventral intermediate thalamic nucleus for the MR-guided focused ultrasound is crucial for enhancing treatment efficacy and avoiding undesirable side effects. In this study, we tested the hypothesis that the spatial relationships between Thalamus Optimized Multi Atlas Segmentation derived segmentations and the post-focused ultrasound lesion can predict post-operative side effects in patients treated with MR-guided focused ultrasound.

MATERIALS AND METHODS: We retrospectively analyzed 30 patients (essential tremor, n = 26; tremor-dominant Parkinson's disease, n = 4) who underwent unilateral ventral intermediate thalamic nucleus focused ultrasound treatment. We created ROIs of coordinate-based indirect treatment target, focused ultrasound-induced lesion, and thalamus and ventral intermediate thalamic nucleus segmentations. We extracted imaging features including 1) focused ultrasound-induced lesion volumes, 2) overlap between lesions and thalamus and ventral intermediate thalamic nucleus segmentations, 3) distance between lesions and ventral intermediate thalamic nucleus segmentation and 4) distance between lesions and the indirect standard target. These imaging features were compared between patients with and without post-operative gait/balance side effects using Wilcoxon rank-sum test. Multi-variate prediction models of side effects based on the imaging features were evaluated using the receiver operating characteristic analyses.

RESULTS: Patients with self-reported gait/balance side effects had a significantly larger extent of focused ultrasound-induced edema, a smaller fraction of the lesion within the ventral intermediate thalamic nucleus segmentation, a larger fraction of the off-target lesion outside the thalamus segmentation, a more inferior centroid of the lesion from the ventral intermediate thalamic nucleus segmentation, and a larger distance between the centroid of the lesion and ventral intermediate thalamic nucleus segmentation ($p < 0.05$). Similar results were found for exam-based side effects. Multi-variate regression models based on the imaging features achieved areas under the curve of 0.99 (95% CI: 0.88 to 1.00) and 0.96 (95% CI: 0.73 to 1.00) for predicting self-reported and exam-based side effects, respectively.

CONCLUSIONS: Thalamus Optimized Multi Atlas Segmentation-based patient-specific segmentation of the ventral intermediate thalamic nucleus can predict post-operative side effects, which has implications for aiding the direct targeting of MR-guided focused ultrasound and reducing side effects.

ABBREVIATIONS: MRgFUS = MR-guided focused ultrasound; ET = essential tremor; PD = Parkinson's disease; VIM = ventral intermediate nucleus; AC-PC = anterior commissure-posterior commissure; FGATIR = Fast Gray Matter Acquisition T1 Inversion Recovery; THOMAS = THalamus Optimized Multi Atlas Segmentation; TH = thalamus; FTM = Fahn-Tolosa-Marín Clinical Rating Scale for Tremor; AUC = areas under the curve.

Received month day, year; accepted after revision month day, year.
From the UCLA Brain Tumor Imaging Laboratory, Center for Computer Vision and Imaging Biomarkers (S.O., A.K., B.M.E., J.Y.), Department of Bioengineering, Henry Samueli School of Engineering and Applied Science (A.K., B.M.E., J.Y.), University of California Los Angeles, Los Angeles, CA, USA; Department of Radiological Sciences (S.O., N.S., B.M.E., J.Y.), Department of Neurosurgery (X.R.S, Z.R., B.M.E., A.A.B.), Department of Neurology (K.A.C., K.A.F.), and Department of Psychiatry and Biobehavioral Sciences (B.M.E.), David Geffen School of Medicine, University of California Los Angeles, Los Angeles, CA, USA.

The authors declare no conflicts of interest related to the content of this article.

Jingwen Yao, PhD, Departments of Radiological Sciences, David Geffen School of Medicine, University of California Los Angeles, 924 Westwood Blvd., Suite 615 Los Angeles, CA 90024, USA; jingwenyao@mednet.ucla.edu

SUMMARY SECTION

PREVIOUS LITERATURE: VIM-MRgFUS is an effective treatment for tremor in patients with essential tremor or Parkinson's disease. Precise targeting of the VIM is crucial but challenging due to its invisibility on standard MR imaging. While indirect targeting using the AC-PC line is common, it does not account for individual anatomical differences. Recently, the THOMAS method, an automated thalamic nucleus segmentation technique based on white-matter-nulled MRI, was developed. We seek to investigate its utility in predicting post-procedural side effect.

KEY FINDINGS: Spatial relationships between FUS-induced lesions and THOMAS-based thalamic segmentations can predict post-

Copyright 2024 by American Society of Neuroradiology.

operative gait and balance side effects. Larger off-target lesion fraction and inferior displacement of lesion centroids relative to VIM were associated with increased side effects. Multivariate models using these imaging features achieved high predictive accuracy for side effects.

KNOWLEDGE ADVANCEMENT: This study provides quantitative evidence that THOMAS-based segmentation can be used for more precise VIM targeting in MRgFUS procedures, offering a objective and reliable method for VIM targeting and intra-operative adjustment. This advancement has significant implications for improving surgical outcomes and reducing post-operative side effects.

INTRODUCTION

MR-guided focused ultrasound (MRgFUS) provides an incisionless therapeutic option for neurological disorders, utilizing high intensity ultrasound waves to ablate target tissue via thermocoagulation[1-4]. Clinically validated for its efficacy and safety[2, 5, 6], MRgFUS has received FDA approval for managing essential tremor (ET) and tremor-dominant Parkinson's disease (PD), two prevalent movement disorders that substantially impact patients' quality of life. For patients with drug resistant tremor, MRgFUS targeting ventral intermediate nucleus (VIM) [4, 7] provides a non-surgical, incisionless solution, particularly benefiting the elderly population with PD and ET[1, 8].

Accurate targeting of the VIM is essential for maximizing MRgFUS treatment efficacy and minimizing undesirable side effects. However, challenges arise from the insufficient contrast and poor delineation of the nucleus on standard anatomical MR images. The traditional VIM targeting relies on indirect targeting based on coordinates relative to the anterior commissure-posterior commissure (AC-PC) line. This technique, while widely adopted, has the limitation of lacking patient-specific anatomical consideration, such as age-related ventricle enlargement[9], which may directly alter the patient-specific VIM coordinates in relationship with the AC-PC line. The VIM targets are often adjusted based on the ventricle size, but the choice remains subjective[5, 10, 11]. In addition, there is currently no consensus on the coordinates used. Commonly used coordinates are 10.5–15 mm lateral to the midline or 10–11 mm lateral to the ventricular wall for cases with enlarged ventricles, 6 mm posterior to the mid-commissural point or 25 % of AC–PC distance anterior to the PC, and 0–2 mm superior to the AC–PC line[5, 10-12].

Both the size and the location of the FUS-induced lesion have been associated with the incidence of post-procedural adverse effects[13-18]. Gait ataxia and unsteadiness has been reported to be the most common neurological side effect, observed in 44–56% patients immediately after treatment (within 48 hours), 22–38% in the short-term (48 hours–3 months), and persisting in 24–38% of the cases beyond 3 months[19]. The high complication rate was postulated to be associated with the small size of VIM and the close proximity of regions responsible for postoperative ataxia with those associated with clinical benefit. The pronounced prevalence of these adverse effects underscores a critical need for the improvement in MRgFUS planning strategies.

Recent advances in imaging techniques offer great promise in personalized VIM targeting, including tractography-based identification of the dentatorubrothalamic tract using DTI[20, 21], proton density imaging[22], and susceptibility MRI at ultrahigh field strength[23-26]. Additionally, a combination of advanced sequences with the recent development of automated segmentation algorithms may further facilitate treatment planning. Fast Gray Matter Acquisition T1 Inversion Recovery (FGATIR), one of the white matter-nulled contrast sequences has been developed for better visualization of the deep gray matter and intra-thalamic structures with high-resolution, including VIM[27-30]. Compared to tractography and susceptibility imaging methods, this method can be acquired without specialized sequences or reconstruction algorithms and can be readily incorporated into the existing clinical protocol. Complementing this imaging technique, the THalamus Optimized Multi Atlas Segmentation (THOMAS) tool has emerged as a novel method for automated delineation of thalamic nuclei[31]. This combination of advanced imaging and an expert-level segmentation tool potentially allows for more precise and personalized MRgFUS treatment planning for the reduction of procedure-related side effects.

This study aims to the integration of FGATIR and THOMAS for patient-specific VIM targeting. We hypothesize that the spatial relationships between post-FUS lesion and THOMAS segmentations will predict the post-operative side effects.

MATERIALS AND METHODS

Patients

We retrospectively analyzed 36 consecutive patients with medication-refractory essential tremor or Parkinson's disease who underwent unilateral VIM MRgFUS at our institution between May 2022 and June 2023. All patients were diagnosed by board-certified neurologists. We excluded six patients with absent or poor-quality pre-operative FGATIR images. Thirty patients were included in the analysis (21 males, age 75.0 ± 8.0 years) (**Online Supplemental Data**). This research was approved by the Institutional Review Board and informed consent was waived for the retrospective study.

Image acquisition

We acquired FGATIR, T1-weighted MPRAGE, and 3D or 2D T2-weighted image for pre-operative scan, either a 3D T1-weighted fast spoiled gradient-echo or a 3D fast imaging employing steady-state acquisition during the operation, and T1-weighted MPRAGE and T2-weighted images for post-operative scan, which were acquired the following day of MRgFUS. Detailed sequence parameters are provided in the **Online Supplemental Data**.

MRgFUS procedure

The therapeutic sonication of the targeted VIM was performed in an MRgFUS system (ExAblate Neuro, InSightec, Tirat Carmel, Israel). Details of the MRgFUS procedure have been described in prior studies[2, 32]. The ablation target coordinate was specified pre-operatively

as one quarter of the length of the AC-PC line from the PC, 14 mm lateral to the midline or 11 mm lateral to third ventricle, and 3 mm superior to the AC-PC line, and fused to intra-operative MR images. Target localization was adjusted further intraoperatively by clinical monitoring of side effects and the reduction of tremor for each patient.

Image post-processing

Five ROIs were generated in patient space for analysis, including the standard treatment target, thalamus segmentation, VIM segmentation, and two FUS lesion segmentations (**Figure 1**). All images were co-registered to the pre-operative T_1-weighted image using an affine transformation in FSL (FLIRT; FMRIB Software Library, Oxford, England; http:// www. fmrib.ox.ac.uk/fsl/) prior to subsequent processing.

Standard FUS target: We generated the spherical ROI of the standard VIM ablation target with a radius of 4 mm centered on the coordinates of the first sonication recorded in the MRgFUS workstation, which was determined by the indirect targeting method based on the AC-PC line as described in the previous paragraph (**Figure 2A**).

FUS lesion segmentations: Pre- and post-operative T_2-weighted images were used to identify FUS-induced lesions. We created the ROIs of Zone A, which includes a strongly hyperintense cytotoxic edema and a central a hypointense coagulation necrosis on T_2-weighted images, and Zone B, which includes the Zone A and the peripheral slightly hyperintense area of vasogenic edema[33-35]. The ROIs were created by subtracting pre-operative T2-weighted images from post-operative T2-weighted images after registration, normalization, and histogram matching. Otsu thresholding method was applied to delineate the ROIs. The detailed procedure is described in the **Online Supplemental Data** and in **Figure 2B**.

THOMAS segmentations: Pre-operative FGATIR images were processed with the THOMAS segmentation tool, a pipeline designed to achieve optimal performance on white matter-nulled imaging contrasts (https://github.com/thalamicseg/thomas_new)[31] to create segmentations of the thalamus (TH) and VIM of the treated side (**Figure 2C**).

Cohort template construction

We created an MRI template specific for the study population using the Advanced Normalization Tools multivariate template construction algorithm (*antsMultivariateTemplateConstruction*)[36]. For each subject, the ROIs generated in previous steps were nonlinearly aligned to the population-specific template to enable direct comparisons across the subjects (**Figure 1**). The details of template creation and the figure of THOMAS segmentations on cohort template images are included in the **Online Supplemental Data**.

Imaging features

We calculated the following imaging features: spatial relationships of ROI centroids (anterior-posterior [AP], right-left [RL], superior-inferior [SI] and absolute distances), overlap/off-target volume of FUS lesions with THOMAS segmentations, and lesion volume characteristics (**Figure 1**). Details are documented in the Online Supplemental Data.

Clinical assessment

We reviewed the clinical records of self-reported and examination-based gait or balance disturbance on the day after MRgFUS and self-reported gait or balance disturbance at one-month post-procedure. The record of self-reported side effects at one month after surgery was not available for one patient. In order to assess the relationships between imaging features and treatment efficacy, we evaluated post-treatment Fahn-Tolosa-Marín Clinical Rating Scale for Tremor (FTM) scores of the treated side on the day after MRgFUS, and the reduction in drawing test scores from before to after the procedure, both of which were evaluated in the operating room. Details are documented in the **Online Supplemental Data**.

Statistical analysis

We compared imaging features between patients with side effects and those without using Wilcoxon rank-sum test. Voxel-wise analysis was performed using a chi-square test to determine if the proportion of subjects with a Zone A lesion in that voxel differed between patients with and without side effects. In addition, we built multi-variate prediction models of self-reported / exam-based side effects using three imaging features that showed the largest z-statistics in cross-sectional comparisons. We further evaluated models using features associated solely with THOMAS segmentations and lesion core (Zone A), to assess the potential of THOMAS segmentations for guiding the ablation procedure. The classification performance of the models was evaluated using the receiver operating characteristic curve analyses. Comparison of imaging features was also performed between patients with no side effects or with side effects that resolved within one month and those with persistent side effects after one month. Lastly, we assessed correlations between imaging features and FTM scores using Spearman's rank correlation. Benjamini-Hochberg (BH) correction was performed for multiple comparison and correlation tests. $P < 0.05$ after BH correction was considered statistically significant.

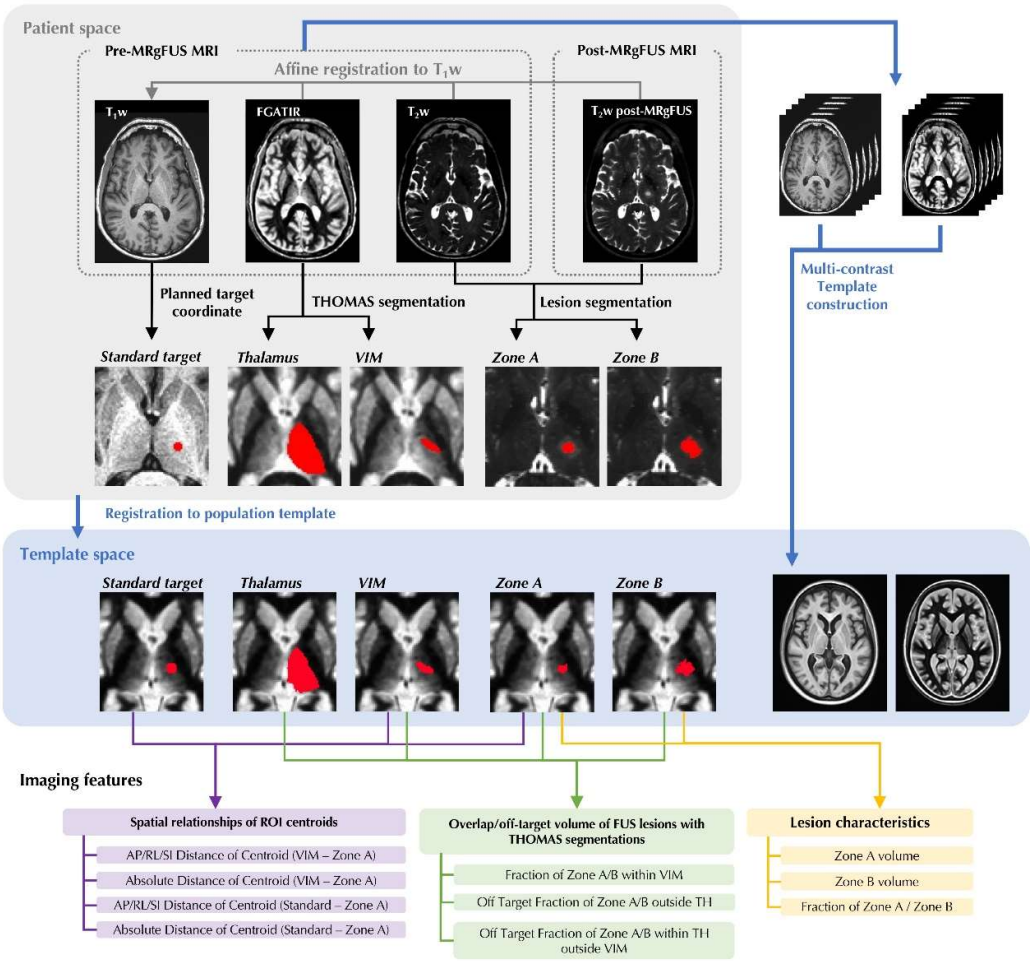

FIG 1. Imaging feature extraction pipeline. ROIs of standard target, FUS lesions and THOMAS segmentations were registered to the population-specific template generated from pre-operative T1-w and FGATIR images. Spatial relationships of ROI centroids, overlap of FUS lesions with segmentations and lesion volume characteristics were assessed. MRgFUS, MR-guided focused ultrasound; FGATIR, Fast Gray Matter Acquisition T1 Inversion Recovery; THOMAS, THalamus Optimized Multi Atlas Segmentation; VIM, ventral intermediate; TH, thalamus; AP, anterior-posterior; RL, right-left, SI, superior-inferior; ROI, region of interest.

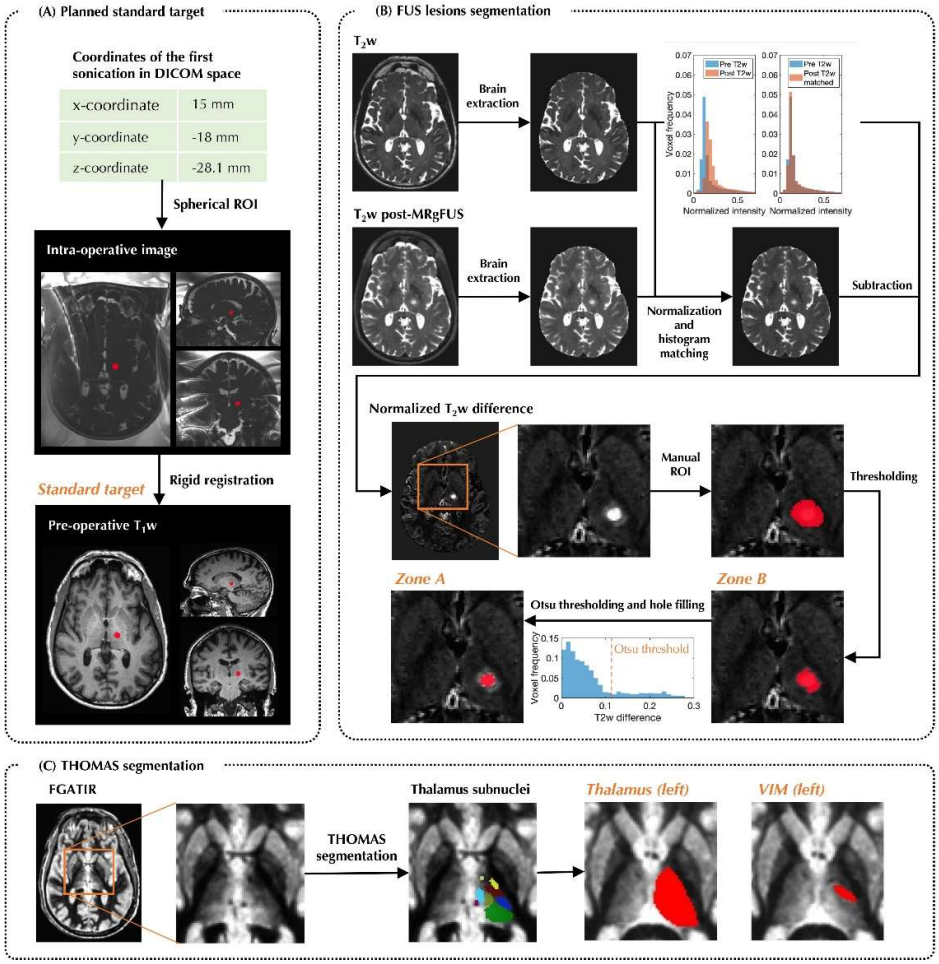

FIG 2. Procedures to create standard target, FUS lesions and THOMAS segmentations of thalamus and VIM. (A) Standard target ROIs were created from coordinates of the first sonication. (B) FUS lesions were generated by subtracting the pre-operative T2-weighted image from the post-operative image and applying a thresholding method. (C) The thalamus and VIM were segmented by applying THOMAS to pre-operative FGATIR images. The VIM here corresponds to the ventral part (inferior half) of the ventral lateral posterior nucleus in the Morel atlas. MRgFUS, MR-guided focused ultrasound; THOMAS, THalamus Optimized Multi Atlas Segmentation; VIM, ventral intermediate; FGATIR, Fast Gray Matter Acquisition T1 Inversion Recovery; ROI, region of interest.

RESULTS

All patients demonstrated marked tremor improvement as suggested by low post-operative tremor scores and patients' self-report. Eighteen patients reported gait or balance disturbance on the day following MRgFUS procedure, with seven exhibiting these disturbances based on physical examination. One of these patients showed lower extremity weakness, while the others displayed gait instability or imbalance. Five out of 18 patients reported symptoms persisting after one month. Detailed clinical evaluations for each patient are provided in the **Online Supplemental Data**.

Example ROIs from two subjects are illustrated in **Figure 3**, depicting the FUS lesions and THOMAS segmentations, as well as their spatial relationships. In the patient with the gait and balance side effects, the FUS lesion extended further outside of the thalamus and VIM segmentations, compared to the patient without side effects. **Figure 4** illustrates THOMAS-based thalamic nuclei segmentations, Zone A probabilistic maps, and standard targets of all subjects and subjects with or without side effects in the population-specific template space, and the result of voxel-wise analysis. Visually, the lesions in the group of patients with side effects were shifted more laterally and inferiorly relative to the VIM. The voxel-wise analysis indicates that voxels outside the VIM segmentation tend to have a higher proportion of patients with side effects compared to those without. The comparison of imaging features between patients with and without side effects are summarized in **Table 1** and the **Online Supplemental Data**. Based on FUS lesion analysis, Zone B volume was significantly larger in patients with self-reported side effects (1.67±0.70 ml vs. 1.04±0.34 ml, $p_{uncorrected} = 0.01$, $p_{BH} = 0.03$). The fraction of Zone A / Zone B was smaller in both patients with self-reported side effects (0.20±0.07 vs. 0.26±0.07, $p_{uncorrected} = 0.01$, $p_{BH} = 0.03$) and those with physical exam-based side effects compared to patients without (0.18±0.05 vs. 0.24±0.08, $p_{uncorrected} = 0.04$), although the difference with physical exam-based side effects was not significant after BH correction.

We found that the volume fraction in Zone A or B overlapping with VIM was significantly smaller in patients with self-reported side effects (**Figure 5A**; Zone A within VIM: 0.31±0.14 vs. 0.50±0.17, $p_{uncorrected} = 0.006$, $p_{BH} = 0.02$; Zone B within VIM: 0.14±0.07 vs. 0.23±0.07, $p_{uncorrected} = 0.001$, $p_{BH} = 0.005$). Similarly, these measurements also trended smaller in patients with physical exam-based side

effects, albeit without statistical significance after BH correction (**Figure 5D**; Zone A within VIM: 0.27±0.12 vs. 0.43±0.18, $p_{uncorrected}$ = 0.03; Zone B within VIM: 0.11±0.05 vs. 0.20±0.08, $p_{uncorrected}$ = 0.01). The off-target lesion volume fractions outside TH positively correlated with the presence of side effects, with higher off-target fractions found in patients with self-reported side effects (**Figure 5B;** Zone A outside TH: 0.33±0.22 vs. 0.09±0.07, $p_{uncorrected}$ < 0.001, p_{BH} = 0.004; Zone B outside TH: 0.52±0.13 vs. 0.27±0.08, $p_{uncorrected}$ < 0.001, p_{BH} < 0.001). The same features were also higher in patients with physical exam-based side effects (**Figure 5E;** Zone B outside TH: 0.57±0.14 vs. 0.38±0.15, $p_{uncorrected}$ = 0.003, p_{BH} = 0.04). There was no significant difference in imaging features between patients with and without persistent side effects at one month after BH multiple comparison correction, although our data showed a trend where patients with persistent side effects showed a smaller fraction of Zone B overlapping with VIM and larger off-target fraction of Zone A or B outside TH compared to those without or with side effects that resolved at one month ($p_{uncorrected}$ < 0.05).

As for the spatial relationships between FUS lesions and THOMAS segmentations, the centroid of Zone A tended to be more posterior, lateral and inferior in patients with self-reported side effects compared to those without, although only superior-inferior direction showed statistical significance (SI distance -2.77±1.43 mm vs. -1.14±0.96 mm, $p_{uncorrected}$ < 0.001, p_{BH} = 0.007). Absolute distance between the centroids of Zone A and the VIM was significantly larger in patients with self-reported side effects (3.79±1.33 mm vs. 2.55±0.83 mm, $p_{uncorrected}$ < 0.001, p_{BH} = 0.02). Absolute distance between the centroids of Zone A and the VIM was also higher in patients with exam-based side effect, although not significant after BH correction (4.20±1.35 mm vs. 3.01±1.17 mm, $p_{uncorrected}$ = 0.04). As for the distance between FUS lesions and the standard planned FUS target, patients with physical exam-based side effects showed Zone A in a more posterior position relative to standard FUS target compared to those without side effects (-0.39±0.69 mm vs. 0.63±0.71 mm, $p_{uncorrected}$ = 0.005). Plots of VIM and lesion centroids for patients with and without side effects in the population-specific template space are depicted in the **Online Supplemental Data**.

Multi-variate regression models using the three most differentiating imaging features were established to predict side effects. The selected imaging features for predicting self-reported side effects include off-target fractions of Zone A/B outside TH, and off-target fraction of Zone B outside VIM and within TH. The multivariate model achieved the area under the curve (AUC) of 0.99 (95% CI: 0.88–1.00) with sensitivity of 100% and specificity of 92% (**Figure 5C**). For predicting physical exam-based side effects, the selected features include off-target fractions of Zone B outside TH, fractions of Zone B within VIM, and AP distance between the centroids of Zone A and standard coordinate. Similarly, the multivariate model achieved high AUC of 0.96 (95% CI: 0.73–1.00) with sensitivity of 86% and specificity of 100% (**Figure 5F**). Multi-variate models using only the imaging features based on the spatial relationships between THOMAS segmentations and Zone A achieved AUC of 0.91 (95% CI: 0.71–0.99, sensitivity 72%, specificity 100%) for identifying patients with self-reported side effects and AUC of 0.78 (95% CI: 0.59–0.93, sensitivity 100%, specificity 65%) for identifying patients with physical exam-based side effects.

The results of of the correlation between imaging features and tremor control, using post-operative tremor score and the reduction in drawing scores after MRgFUS, are shown in the **Online Supplemental Data**. Although no significant correlation between imaging features and FTM scores were found after BH multiple statistics correction, lower positioning of Zone A relative to the VIM showed a tendency to correlate with a lower post-operative tremor score and a greater reduction in drawing score.

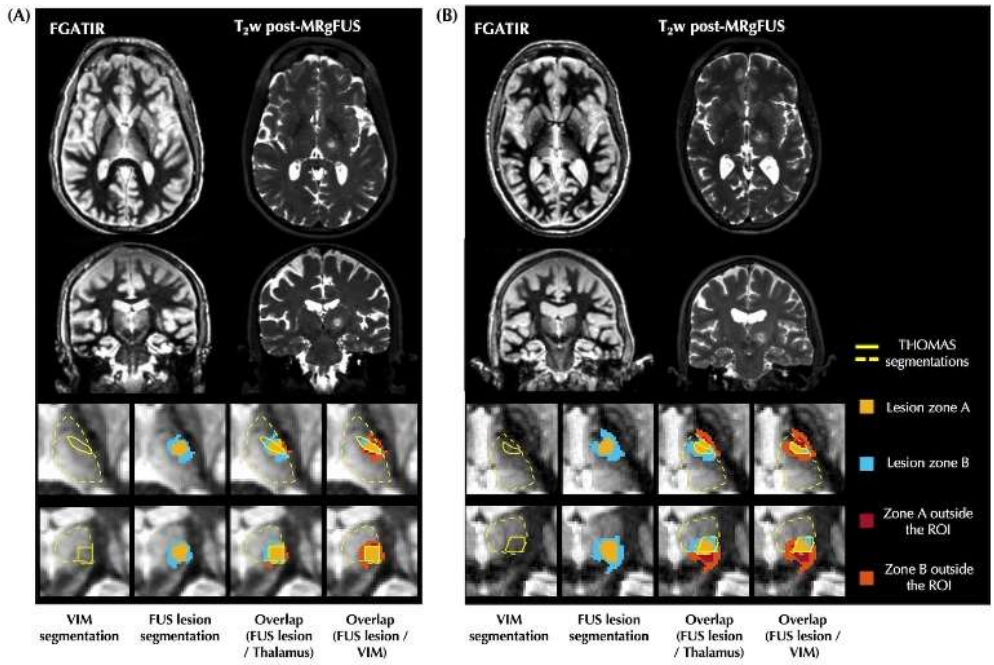

FIG 3. Example THOMAS segmentations (yellow line: thalamus; white line: VIM nucleus) and MRgFUS treated lesions (magenta: Zone A; cyan: Zone B) are shown in axial and coronal views. In the patient with side effects (A), lesions extend farther out of the thalamus and segmented VIM, compared to the patient without side effects (B). FGATIR, Fast Gray Matter Acquisition T1 Inversion Recovery; MRgFUS, MR-guided focused ultrasound; THOMAS, Thalamus Optimized Multi Atlas Segmentation; VIM, ventral intermediate nucleus; ROI, region of interest.

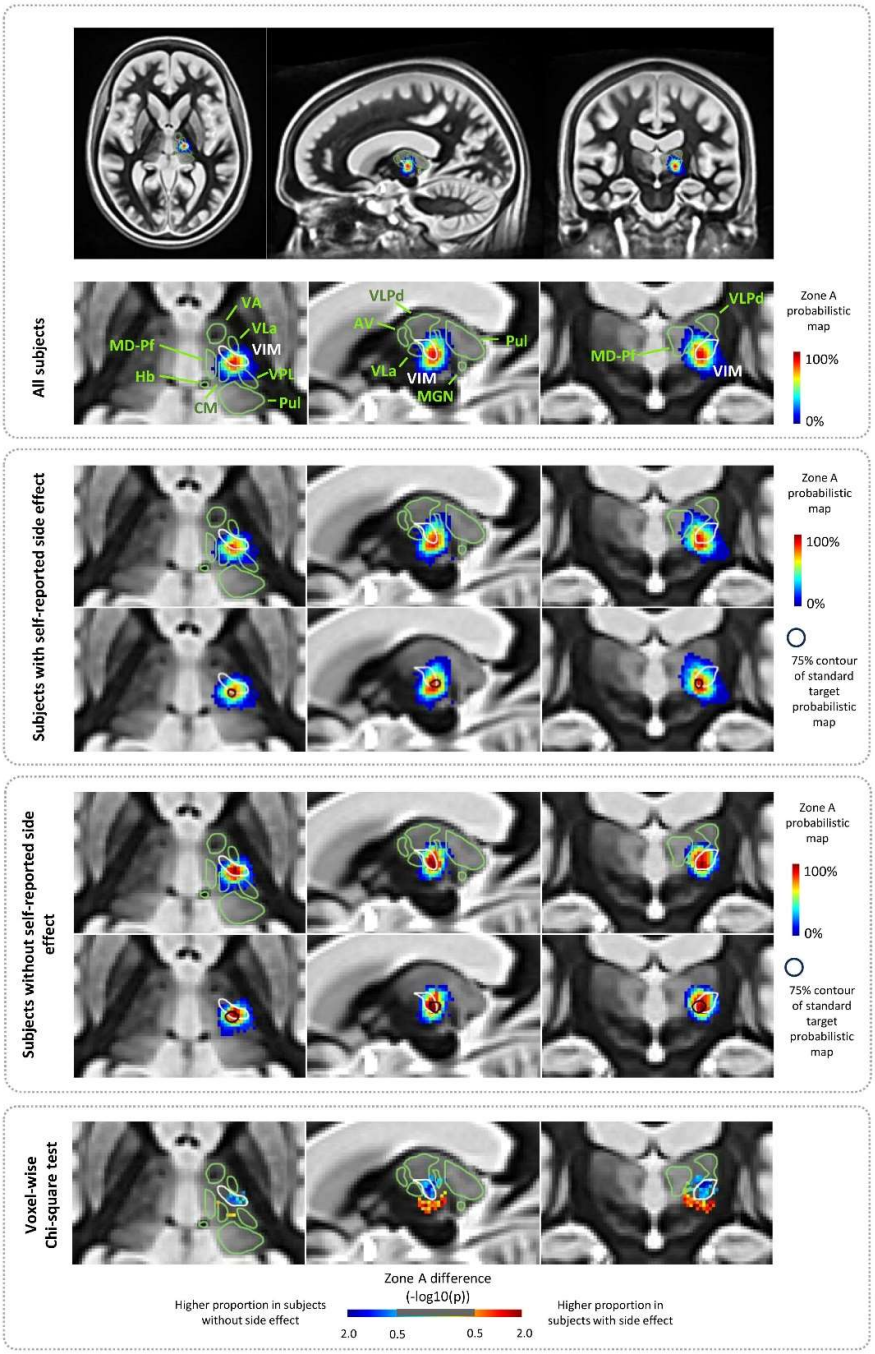

FIG 4. Probabilistic maps of Zone A in the population-specific template space. The spatial relationship between THOMAS-based thalamic nuclei segmentations, Zone A probabilistic maps, and standard targets are illustrated in different cohorts. The Zone A probabilistic map represents the voxel-wise percentage of FUS lesions across the subjects, and the standard target contour represents 75th percentile of standard coordinate ROI across the subjects. THOMAS, THalamus Optimized Multi Atlas Segmentation; FUS, focused ultrasound; VA, ventral anterior nucleus; VLa, ventral lateral anterior nucleus; VLP, ventral lateral posterior nucleus; VPL, ventral posterior lateral nucleus; VPLd, dorsal part of ventral posterior lateral nucleus; Pul, pulvinar nucleus; CM, centromedian nucleus; MD-Pf, mediodorsal-parafascicular nucleus; Hb, habenula; MGN, medial geniculate nucleus; ROI, region of interest.

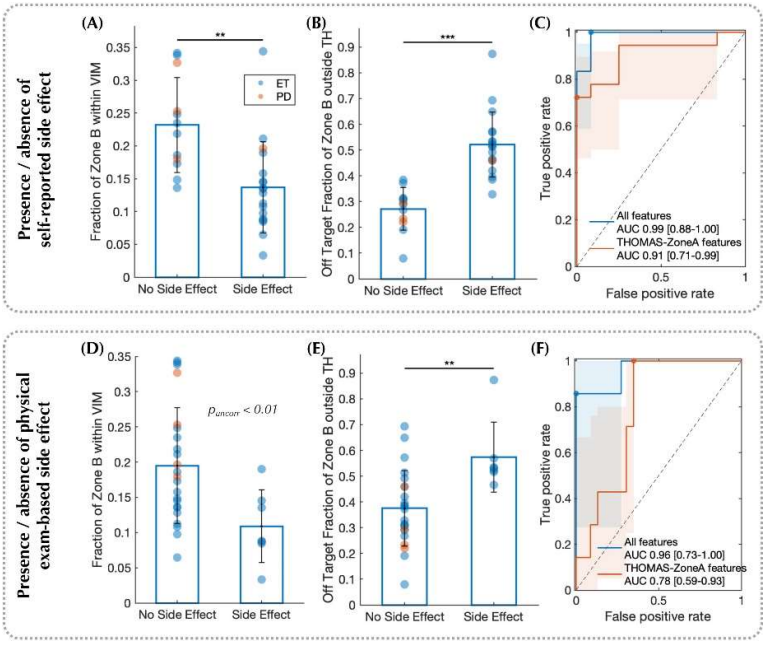

FIG 5. Results of imaging feature comparisons between patients with self-reported or physical exam-based gait/balance side effects and those without. In patients with side effects, Zone B shows less overlap with VIM segmentation and the off-target fraction of Zone B outside TH segmentation is greater (Graphs A-B and D-E). Graphs C and F show receiver operating characteristic curves of multi-variate prediction models of side effects using imaging features. ET, essential tremor; PD, Parkinson's disease; VIM, ventral intermediate; TH, thalamus; AUC, area under the curve.

DISCUSSION

To examine the usefulness of FGATIR in combination with the thalamus segmentation algorithm, THOMAS, on improving VIM MRgFUS precision, we retrospectively assessed the relationships between FUS lesions, THOMAS segmentations derived from pre-FUS images, and the conventional target adopted during FUS procedures in 30 ET and tremor-dominant PD patients. Two main results emerged from our study: (1) patients with post-FUS gait and balance side effect exhibit significantly different spatial relationships between FUS lesions and THOMAS-based segmentations compared to those without; (2) multivariate models based on imaging characteristics of FUS lesions and THOMAS segmentations demonstrated high predictive accuracy for post-procedural side effects.

Our findings align with previous research[6, 13, 37], indicating that a larger volume of Zone B and a smaller fraction of Zone A/Zone B – indicative of a greater extent of vasogenic edema – are associated with gait and balance side effects. One potential explanation is that the larger area of vasogenic edema may lead to the disruption of the corticospinal and/or cerebellothalamic tracts. In addition to the adjustments to the duration and temperature of sonication during the procedure, hardware improvement to reduce the size of lesions could be an effective approach to minimizing side effects, while it is necessary to consider that excessively small lesions may lead to insufficient therapeutic efficacy [38].

Our results also showed that patients with acute gait and balance side effects exhibited a significantly smaller fraction of Zone A or Zone B within VIM and a larger off-target lesion fraction outside TH, alongside a greater distance between Zone A and VIM. Although only superior-inferior direction showed statistical significance, there was a trend for the centroid of Zone A to be more posterior, lateral and inferior relative to the VIM, supporting previous evidence that lesions inferolateral to the thalamus were associated with an increased risk of acute adverse effects on gait and dysmetria[13, 37, 39]. These results are associated with the finding that gait difficulties occur due to lesions impacting the corticospinal tract, which is located just lateral to theVIM[13, 21]. Our results add to the existing literature reporting lesion location as a significant factor impacting post-FUS side effect, and provides evidence that such off-target effects can be quantitatively evaluated using imaging features retrieved with a semi-automated processing procedure. These findings also highlight the utility of THOMAS-based segmentations in refining targets to reduce the acute side effects of MRgFUS. As demonstrated in previous literature, the dentato-rubro-thalamic tract, which is relayed by the VIM nucleus, also contributes to gait side effects. Therefore, even if the VIM is precisely targeted, side effects are still considered to occur with suboptimal size and temperature of the lesion [13]. This explains the overlap in the locations of FUS lesions between patients with and without gait side effects in our study, as shown in **Figure 5** and **Supplementary Figure 2**.

Among the 18 patients experiencing acute side effects post-MRgFUS, five reported persistent side effects one month later, a slightly lower incidence rate than previously reported[19]. No significant differences were found in imaging features between patients with and without persistent side effects after BH correction. However, trends toward significance were observed in the overlap of Zone A/B with the VIM and the off-target Zone A/B fraction outside the thalamic segmentation. Given that post-FUS lesion decreases over time and lesion shrinkage varies among individuals, future studies incorporating long-term follow-up MR imaging may assist the identification of specific imaging characteristics associated with persistent side effects.

THOMAS was developed using manual segmentations of 7T white matter-nulled MPRAGE data guided by the Morel atlas[31, 40]. Similar

to white matter-nulled MPRAGE, FGATIR provides improved intra-thalamic contrast by highlighting grey matter structures that are surrounded by highly myelinated areas using preferential nullification of white matter signal[30]. Such unique contrast is thought to contribute to the reliability of THOMAS segmentation, as validated by high Dice coefficient scores when compared to the ground truth segmentation by expert neuroradiologist[31]. The VIM segmentation obtained using THOMAS on pre-operative images can effectively guide target selection for pre-operative planning and assist with intra-operative adjustments. Despite its great potential, the clinical application of THOMAS in direct VIM targeting for neuromodulatory treatments like deep brain stimulation or MRgFUS has been scarcely evaluated. Notably, a recent study using THOMAS on 7T MRI found no correlations between overlap/spatial relationships of ablation lesions with VIM and 1-month post-treatment clinical outcome[17], which is consistent with our results. Expanding upon existing research, our study explores the link between FUS-induced imaging characteristics and side effects using THOMAS with 3T MR images. While it is an expected finding that post-procedural side effects are associated with off-target ablation, our study provides rigorous quantitative evidence supporting this hypothesis. Additionally, the integration of FGATIR and THOMAS in our methodology can serve as a practical tool for objective and reproducible localization of VIM, for both pre-operative planning and intra-operative adjustments, reducing the reliance on neurosurgeons' experience and expertise.

There have been increasing efforts to improve the targeting of VIM for neuromodulation using various advanced imaging methods[1, 21, 41]. VIM targets based on patient-specific dentatorubrothalamic tracts demonstrated by DTI were more anterior and medial than the indirect methods, which may help avoid regions at risk for motor and sensory adverse effects, and VIM targeting by DTI showed reduced post-procedure acute ataxia as compared to indirect targeting[19, 42]. Compared to tractography-based methods, segmenting FGATIR images using THOMAS offers several advantages. First, FGATIR has a higher resolution (about 1-mm isotropic) than DTI (about 2-mm isotropic). Second, FGATIR is less susceptible to image distortion compared to DTI[43]. Tractography based on DTI data may also suffer from inadequate representation of the underlying anatomy in areas with crossing fibers and within gray matter structures such as the thalamus[44, 45]. As such, its usefulness as the primary method of VIM targeting are still being debated[46]. Other direct VIM imaging methods include susceptibility weighted imaging[23, 25, 26] and quantitative susceptibility mapping[24], which have only been evaluated at ultrahigh field of 7T, but not at the more clinically-accessible field strength of 3T or lower. On the other hand, the THOMAS segmentation method we evaluated provides reliable high-resolution targeting of VIM using clinically available FGATIR images acquired by 3T MRI.

MRgFUS is influenced by various factors beyond targeting, such as low skull density ratios, which require higher energy to reach therapeutic temperatures [47]. Additionally, thermal ablation lesions in the focal zone form a prolate ellipsoid shape [48]. Techniques like CT-based aberration correction and echo focusing have been developed to stabilize lesion formation, but further research is needed to confirm their full effectiveness [47].

Our study has several limitations. First, a systematic pre-operative and long-term follow up tremor and side effect evaluations were not available. More rigorously controlled studies with adequate pre- and long-term tremor scores are necessary to evaluate the impact of VIM segmentation by THOMAS on tremor improvement and persistent side effects. Furthermore, although we performed the additional analysis using physical exam-based gait and balance assessment to overcome the subjective bias of self-reported side effects, prospective studies of MRgFUS-associated side effect using quantitative measures such as Berg Balance Scale and standardized pre- and post-procedure neurologic exam protocols will provide a more comprehensive and robust evaluation of gait and balance impairment. Such methods are particularly crucial for ET and PD, which are prone to causing gait disturbances. Second, due to the limited number of patients, we did not assess other side effects including sensory and speech symptoms. While less common than gait disturbance, these side effects are critical for patients' quality of life[13, 42]. Lastly, the relatively small difference of distance observed between the two groups compared to MRI resolutions indicates that the precise targeting of VIM would benefit from techniques with improved imaging resolution. Future developments to enhance MRI resolution, including ultrahigh field MRI and super-resolution deep learning approaches may further enhance the accuracy of THOMAS for direct targeting.

Table 1: Comparisons of imaging features between patients with and without side effect.

		Self-reported side effect		Physical exam-based side effect
	MRI Features	**Gait/balance**	**Gait/balance > 1 month**	**Gait/balance**
		p-value	*p-value*	*p-value*
FUS lesion volume	Volume of Zone A	0.21	0.31	0.96
	Volume of Zone B	**0.01**	0.15	0.14
	Fraction of Zone A / Zone B	**0.01**	0.45	0.04
Overlap between FUS lesions and THOMAS segmentations	Fraction of Zone A within VIM*	**0.006**	0.09	0.03
	Fraction of Zone B within VIM*	**0.001**	0.01	0.01
	Off Target Fraction of Zone A outside TH**	**< 0.001**	0.02	0.02
	Off Target Fraction of Zone B outside TH**	**< 0.001**	0.008	**0.003**

Distance between FUS core lesion and THOMAS segmentations	Off Target Fraction of Zone A within TH***	0.57	0.22	1
	Off Target Fraction of Zone B within TH***	**< 0.001**	0.07	0.05
	AP Distance of Centroid (VIM - Zone A)	0.57	0.45	0.52
	RL Distance of Centroid (VIM - Zone A)	0.49	0.52	0.34
	SI Distance of Centroid (VIM - Zone A)	**< 0.001**	0.27	0.1
	Absolute Distance of Centroid (VIM - Zone A)	**< 0.001**	0.19	0.04
Distance between FUS core lesion and standard coordinate	AP Distance of Centroid (Standard - Zone A)	0.64	0.32	**0.005**
	RL Distance of Centroid (Standard - Zone A)	0.17	0.94	0.74
	SI Distance of Centroid (Standard - Zone A)	0.43	0.69	0.7
	Absolute Distance of Centroid (Standard - Zone A)	0.23	0.65	0.7

Note:

*: Volume of overlap between Zone A (or B) and VIM divided by that of Zone A (or B).

**: Volume of Zone A (or B) outside TH divided by that of Zone A (or B).

***: Volume of Zone A within TH but outside VIM divided by that of Zone A (or B).

P-values in the table represent uncorrected *p*-values. The bolded items represent statistical tests with Benjamini–Hochberg corrected *p*-values < 0.05.

Abbreviations: FUS, focused ultrasound; THOMAS, THalamus Optimized Multi Atlas Segmentation; VIM, ventral intermediate; TH, thalamus; AP, anterior-posterior; RL, right-left, SI, superior-inferior.

CONCLUSIONS

In conclusion, THOMAS segmentation derived imaging features predicts post-operative gait/balance side effect in patients treated with VIM MRgFUS, and may provide a potential tool for aiding the direct targeting of VIM and reducing side effects in patients undergoing MRgFUS.

ACKNOWLEDGMENTS

S.O. is grateful for the scholarship support from the Nakatani Foundation.

REFERENCES

1. Bruno F, Catalucci A, Arrigoni F, et al. An experience-based review of HIFU in functional interventional neuroradiology: transcranial MRgFUS thalamotomy for treatment of tremor. Radiol Med 2020;125:877-886
2. Elias WJ, Lipsman N, Ondo WG, et al. A Randomized Trial of Focused Ultrasound Thalamotomy for Essential Tremor. N Engl J Med 2016;375:730-739
3. Jolesz FA. MRI-guided focused ultrasound surgery. Annu Rev Med 2009;60:417-430
4. Yamamoto K, Sarica C, Loh A, et al. Magnetic resonance-guided focused ultrasound for the treatment of tremor. Expert Rev Neurother 2022;22:849-861
5. Elias WJ, Huss D, Voss T, et al. A pilot study of focused ultrasound thalamotomy for essential tremor. N Engl J Med 2013;369:640-648
6. Wintermark M, Druzgal J, Huss DS, et al. Imaging findings in MR imaging-guided focused ultrasound treatment for patients with essential tremor. AJNR Am J Neuroradiol 2014;35:891-896
7. Quadri SA, Waqas M, Khan I, et al. High-intensity focused ultrasound: past, present, and future in neurosurgery. Neurosurg Focus 2018;44:E16
8. de Rijk MC, Breteler MM, Graveland GA, et al. Prevalence of Parkinson's disease in the elderly: the Rotterdam Study. Neurology 1995;45:2143-2146
9. Jochems ACC, Muñoz Maniega S, Del CVHM, et al. Contribution of white matter hyperintensities to ventricular enlargement in older adults. Neuroimage Clin 2022;34:103019
10. Børretzen MN, Bjerknes S, Sæhle T, et al. Long-term follow-up of thalamic deep brain stimulation for essential tremor - patient satisfaction and mortality. BMC Neurol 2014;14:120
11. Peters J, Maamary J, Kyle K, et al. Outcomes of Focused Ultrasound Thalamotomy in Tremor Syndromes. Mov Disord 2024;39:173-182
12. Obwegeser AA, Uitti RJ, Witte RJ, et al. Quantitative and qualitative outcome measures after thalamic deep brain stimulation to treat disabling tremors. Neurosurgery 2001;48:274-281; discussion 281-274
13. Boutet A, Ranjan M, Zhong J, et al. Focused ultrasound thalamotomy location determines clinical benefits in patients with essential tremor. Brain 2018;141:3405-3414

14. Bruno F, Catalucci A, Varrassi M, et al. Comparative evaluation of tractography-based direct targeting and atlas-based indirect targeting of the ventral intermediate (Vim) nucleus in MRgFUS thalamotomy. Sci Rep 2021;11:13538
15. Mohammed N, Patra D, Nanda A. A meta-analysis of outcomes and complications of magnetic resonance-guided focused ultrasound in the treatment of essential tremor. Neurosurg Focus 2018;44:E4
16. Paff M, Boutet A, Germann J, et al. Focused Ultrasound Thalamotomy Sensory Side Effects Follow the Thalamic Structural Homunculus. Neurol Clin Pract 2021;11:e497-e503
17. Su JH, Choi EY, Tourdias T, et al. Improved Vim targeting for focused ultrasound ablation treatment of essential tremor: A probabilistic and patient-specific approach. Hum Brain Mapp 2020;41:4769-4788
18. Yamamoto K, Sarica C, Elias GJB, et al. Ipsilateral and axial tremor response to focused ultrasound thalamotomy for essential tremor: clinical outcomes and probabilistic mapping. J Neurol Neurosurg Psychiatry 2022
19. Agrawal M, Garg K, Samala R, et al. Outcome and Complications of MR Guided Focused Ultrasound for Essential Tremor: A Systematic Review and Meta-Analysis. Front Neurol 2021;12:654711
20. King NKK, Krishna V, Basha D, et al. Microelectrode recording findings within the tractography-defined ventral intermediate nucleus. J Neurosurg 2017;126:1669-1675
21. Sammartino F, Krishna V, King NK, et al. Tractography-Based Ventral Intermediate Nucleus Targeting: Novel Methodology and Intraoperative Validation. Mov Disord 2016;31:1217-1225
22. Wakim AA, Sioda NA, Zhou JJ, et al. Direct targeting of the ventral intermediate nucleus of the thalamus in deep brain stimulation for essential tremor: a prospective study with comparison to a historical cohort. J Neurosurg 2022;136:662-671
23. Abosch A, Yacoub E, Ugurbil K, et al. An assessment of current brain targets for deep brain stimulation surgery with susceptibility-weighted imaging at 7 tesla. Neurosurgery 2010;67:1745-1756; discussion 1756
24. Deistung A, Schäfer A, Schweser F, et al. Toward in vivo histology: a comparison of quantitative susceptibility mapping (QSM) with magnitude-, phase-, and R2*-imaging at ultra-high magnetic field strength. Neuroimage 2013;65:299-314
25. Najdenovska E, Tuleasca C, Jorge J, et al. Comparison of MRI-based automated segmentation methods and functional neurosurgery targeting with direct visualization of the Ventro-intermediate thalamic nucleus at 7T. Sci Rep 2019;9:1119
26. Xiao Y, Zitella LM, Duchin Y, et al. Multimodal 7T Imaging of Thalamic Nuclei for Preclinical Deep Brain Stimulation Applications. Front Neurosci 2016;10:264
27. Grewal SS, Middlebrooks EH, Kaufmann TJ, et al. Fast gray matter acquisition T1 inversion recovery MRI to delineate the mammillothalamic tract for preoperative direct targeting of the anterior nucleus of the thalamus for deep brain stimulation in epilepsy. Neurosurg Focus 2018;45:E6
28. Morishita T, Higuchi MA, Kobayashi H, et al. A retrospective evaluation of thalamic targeting for tremor deep brain stimulation using high-resolution anatomical imaging with supplementary fiber tractography. J Neurol Sci 2019;398:148-156
29. Neudorfer C, Kroneberg D, Al-Fatly B, et al. Personalizing Deep Brain Stimulation Using Advanced Imaging Sequences. Ann Neurol 2022;91:613-628
30. Sudhyadhom A, Haq IU, Foote KD, et al. A high resolution and high contrast MRI for differentiation of subcortical structures for DBS targeting: the Fast Gray Matter Acquisition T1 Inversion Recovery (FGATIR). Neuroimage 2009;47 Suppl 2:T44-52
31. Su JH, Thomas FT, Kasoff WS, et al. Thalamus Optimized Multi Atlas Segmentation (THOMAS): fast, fully automated segmentation of thalamic nuclei from structural MRI. Neuroimage 2019;194:272-282
32. Lipsman N, Mainprize TG, Schwartz ML, et al. Intracranial applications of magnetic resonance-guided focused ultrasound. Neurotherapeutics 2014;11:593-605
33. Chen L, Bouley DM, Harris BT, et al. MRI study of immediate cell viability in focused ultrasound lesions in the rabbit brain. J Magn Reson Imaging 2001;13:23-30
34. Ghanouni P, Pauly KB, Elias WJ, et al. Transcranial MRI-Guided Focused Ultrasound: A Review of the Technologic and Neurologic Applications. AJR Am J Roentgenol 2015;205:150-159
35. Ram Z, Cohen ZR, Harnof S, et al. Magnetic resonance imaging-guided, high-intensity focused ultrasound for brain tumor therapy. Neurosurgery 2006;59:949-955; discussion 955-946
36. Tustison NJ, Cook PA, Holbrook AJ, et al. The ANTsX ecosystem for quantitative biological and medical imaging. Sci Rep 2021;11:9068
37. Segar DJ, Lak AM, Lee S, et al. Lesion location and lesion creation affect outcomes after focused ultrasound thalamotomy. Brain 2021;144:3089-3100
38. Kapadia AN, Elias GJB, Boutet A, et al. Multimodal MRI for MRgFUS in essential tremor: post-treatment radiological markers of clinical outcome. J Neurol Neurosurg Psychiatry 2020;91:921-927
39. Boutet A, Loh A, Chow CT, et al. A literature review of magnetic resonance imaging sequence advancements in visualizing functional neurosurgery targets. J Neurosurg 2021;135:1445-1458
40. Tourdias T, Saranathan M, Levesque IR, et al. Visualization of intra-thalamic nuclei with optimized white-matter-nulled MPRAGE at 7T. Neuroimage 2014;84:534-545
41. Lehman VT, Lee KH, Klassen BT, et al. MRI and tractography techniques to localize the ventral intermediate nucleus and dentatorubrothalamic tract for deep brain stimulation and MR-guided focused ultrasound: a narrative review and update. Neurosurg Focus 2020;49:E8
42. Ranjan M, Elias GJB, Boutet A, et al. Tractography-based targeting of the ventral intermediate nucleus: accuracy and clinical utility in MRgFUS thalamotomy. J Neurosurg 2019:1-8
43. Zhuang J, Hrabe J, Kangarlu A, et al. Correction of eddy-current distortions in diffusion tensor images using the known directions and strengths of diffusion gradients. J Magn Reson Imaging 2006;24:1188-1193
44. Coenen VA, Varkuti B, Parpaley Y, et al. Postoperative neuroimaging analysis of DRT deep brain stimulation revision surgery for complicated essential tremor. Acta Neurochir (Wien) 2017;159:779-787
45. Yamada K, Sakai K, Akazawa K, et al. MR tractography: a review of its clinical applications. Magn Reson Med Sci 2009;8:165-174
46. Nowacki A, Schlaier J, Debove I, et al. Validation of diffusion tensor imaging tractography to visualize the dentatorubrothalamic tract for surgical planning. J Neurosurg 2018;130:99-108
47. Baek H, Lockwood D, Mason EJ, et al. Clinical Intervention Using Focused Ultrasound (FUS) Stimulation of the Brain in Diverse Neurological Disorders. Front Neurol 2022;13:880814
48. Mattay RR, Kim K, Shah L, et al. MR Thermometry during Transcranial MR Imaging-Guided Focused Ultrasound Procedures: A Review. AJNR Am J Neuroradiol 2023;45:1-8

SUPPLEMENTAL FILES

MATERIALS AND METHODS

Image acquisition

Pre- and post-operative MR images were acquired with 3T scanners (Prisma/Skyra/Vida/TrioTim, Siemens Healthcare, Erlangen, Germany) using 20 channel head and neck coils, while intra-operative images were acquired with a 3T scanner (Signa Architect, GE Healthcare, Chicago, Illinois, USA) using a body transmit/receiver coil. For pre-operative scan, FGATIR, T1-weighted MPRAGE, and 3D or 2D T2-weighted image were acquired. Only T1-weighted MPRAGE and T2-weighted images were acquired in the post-operative scan. Either a 3D T1-weighted fast spoiled gradient-echo or a 3D fast imaging employing steady-state acquisition was acquired during the operation.

Pre-operative images: FGATIR (TE = 2.79–3.52 ms, TR = 3000 ms, FA = 8–9 degrees, TI = 409 ms, resolution = 0.8×0.8×1.0 mm), T_1-weighted MPRAGE (TE = 2.21–3.26 ms, TR = 1840–2300 ms, FA = 8–15 degrees, TI = 900–1100 ms, resolution = 1.0×1.0×1.0 mm) and 3D T_2-weighted image (TE = 108–410 ms, TR = 1000–3200 ms, FA = 120 degrees, resolution = 0.5×0.5×1.0–1.0×1.0×1.0 mm) or 2D axial T_2-weighted TSE (one subject, TE = 108 ms, TR = 5750 ms, FA = 114 degrees, resolution = 0.5×0.5×2.5 mm).

Intra-operative images: 3D T_1-weighted fast spoiled gradient-echo (TE = 3.02–3.09 ms, TR = 7.34–7.45 ms, FA = 120 degrees, resolution = 0.5×0.5×1.7 mm) or 3D fast imaging employing steady-state acquisition (TE = 2.21 ms, TR = 4.67–4.70 ms, FA = 55 degrees, resolution = 0.9×0.9×1.5 mm).

Post-operative images acquired the day after FUS: T_1-weighted MPRAGE and T_2-weighted image (parameters were same as pre-operative images).

Image post-processing

FUS lesion segmentation: Briefly, brain masks were generated using the deep-learning-based brain extraction tool algorithm (https://github.com/MIC-DKFZ/HD-BET) [1] on the pre-operative T_2-weighted image and applied to both images. Next, the brain-extracted T_2-weighted images underwent normalization and histogram matching of image intensity. We then performed a voxel-by-voxel subtraction between normalized T_2-weighted images. Finally, ROIs of Zone B were segmented from manually created ROIs by thresholding the subtraction map, and ROIs of Zone A were further segmented using Otsu's thresholding method[2]. Manual edits of the Zone A and B ROIs were performed if necessary, by SO, a radiologist with 11 years of experience in neuroradiology, and JY with 7 years of experience in neuroimaging research.

Cohort template construction

We created an MRI template specific for the study population using the Advanced Normalization Tools multivariate template construction algorithm (*antsMultivariateTemplateConstruction*) [3]. Specifically, co-registered T1-weighted and FGATIR images from all patients were used in the process, with 4 template construction iterations, cross correlation cost function, greedy SyN nonlinear transformation model, and Montreal Neurological Institute T1-weighted atlas as initial target for input images. For each subject, the ROIs generated in previous steps were nonlinearly aligned to the population-specific template to enable direct comparisons across the subjects, using the deformation fields computed during the registration of individual structural images to the study-specific template. For patients treated on the right VIM, we flipped the images in the left-right direction before using them as input for the template building algorithm.

1. Isensee F, Schell M, Pflueger I, et al. Automated brain extraction of multisequence MRI using artificial neural networks. *Hum Brain Mapp* 2019;40:4952-4964
2. Otsu N. A Threshold Selection Method from Gray-Level Histograms. *IEEE Transactions on Systems, Man, and Cybernetics* 1979;9:62-66
3. Tustison NJ, Cook PA, Holbrook AJ, et al. The ANTsX ecosystem for quantitative biological and medical imaging. *Sci Rep* 2021;11:9068

Imaging features

For the assessment of spatial relationships of ROI centroids, we calculated anterior-posterior (AP), right-left (RL), superior-inferior (SI) and absolute distances of the centroid of Zone A from centroid of the VIM segmentation and from the standard target in the population-specific template space. To evaluate the overlap of the FUS lesions with the THOMAS segmentations, we calculated the fraction of Zone A (or B) within the VIM by dividing the volume of overlap of Zone A (or B) and VIM by that of the Zone A (or B). For off-target fractions outside the TH (or outside VIM and within TH), we divided the off-target volumes of Zone A (or B) by that of Zone A (or B). For lesion characteristics, we measured the volumes of Zone A and Zone B, and the fraction of Zone A / Zone B.

Clinical assessments

While neurologists and neurosurgeons were involved in the scoring and documentation of pre- and post-treatment tremor as part of their clinical assessments, there were variable intervals of score reporting pre- and post-treatment in this retrospective patient cohort. Therefore, we evaluated post-treatment Fahn-Tolosa-Marín Clinical Rating Scale for Tremor (FTM) scores of the treated side on the day after MRgFUS, as a surrogate of treatment efficacy given the consistent availability of these scores in the medical record. We used FTM scores

of the sum of tremor severity (items 1-3) and drawing test (items 11-13) of the treated side (maximum score 24) for analysis. As the handwriting scores were not evaluated for patients whose non-dominant side was treated and the pouring test was not performed in 11 out of the 30 cases, we did not include these sub-scores for the analysis. The record of post-treatment FTM scores on the first day post MRgFUS was not available for one patient. We referred to the records of the pre-operative neurological examinations of patients as well and confirmed the newly observed symptoms as side effects based on these records.

In addition, as another assessment metric, we calculated the reduction in tremor scores from before to after the procedure, both of which were evaluated in the operating room. For this analysis, only drawing test scores were used, as they were the only consistently recorded measurements in the operating room. The drawing score was the sum of the scores for a large spiral, a small spiral and a straight line (maximum score 12; four for each drawing task).

All examinations and documentation of side effects and FTM scores on the first day post-procedure were performed by two neurosurgery nurse practitioners. Neurosurgery nurse practitioners are certified by the American Association of Nurse Practitioners (AANP) and the American Nurses Credentialing Center (ANCC) in addition to receiving at least six months of dedicated clinical training in the neurologic exam as part of the neurosurgical clinical workflow to serve as a neurosurgical nurse practitioner. Self-reported side effects at one month were recorded by neurosurgery nurse practitioners or a board-certified neurosurgeon. The drawing test scores performed in the operation room were evaluated by a board-certified neurologist (K.A.F.).

RESULTS

The mean and standard deviation of post-operative tremor scores were 2.66±2.44, and those of pre- and post-operative drawing score at the operation room were 9.65±2.30 and 2.85±1.66, respectively. Although not significant, moderate positive correlations were observed between the VIM – Zone A centroid SI distance and post-operative FTM scores and the drawing score reduction after operation (**Supplementary Figure 3D**; FTM score: $r = 0.40$, $p_{uncorrected} < 0.05$; drawing score reduction: $r = 0.43$, $p_{uncorrected} < 0.05$), as well as between the standard target – Zone A centroid RL distance and post-operative FTM scores (FTM score: $r = 0.36$, $p_{uncorrected} = 0.06$). In terms of the overlaps between FUS lesions and THOMAS segmentations, off-target fraction of Zone B outside VIM and within TH was found to be moderately correlated with post-FUS FTM scores (**Supplementary Figure 3C**; FTM score: $r = 0.42$, $p_{uncorrected} < 0.05$; drawing score reduction: $r = 0.36$, $p_{uncorrected} = 0.07$). The other imaging features, including the Zone A volume and the fraction of Zone A within VIM were found to have weak or no correlation with the clinical tremor assessments (**Supplementary Figure 3A, B**).

TABLES AND FIGURES

Supplementary Table 1: Patient characteristics (n = 30).

Characteristic	
Age, mean ± SD (years)	75.0 ± 8.0
Sex, Male/Female	21/9
Disease, ET/PD	26/4
Dominant hand, Right/Left	27/3
Treated side, Dominant/Non-dominant hand	27/3
Disease duration, mean ± SD (years)	24.7 ± 21.7

Abbreviations: SD, standard deviation; ET, essential tremor; PD, Parkinson's disease.

Supplementary Table 2: Clinical information of each patient.

Patient No.	Age at FUS (years)	Sex	Dominant hand	Diagnosis	Self-reported side effect*	Self-reported side effect after 1 month	Exam-based side effect	Pre-FUS drawing score**	Post-FUS drawing score**	Post-FUS FTM score***
1	77	F	R	ET	+	+	-	7	3	3
2	68	M	R	ET	+	n/a	-	12	3	4
3	77	M	R	ET	+	+	-	11	6	7
4	65	M	R	ET	+	-	+	12	3	0
5	83	M	R	ET	+	-	+	11	2	1
6	50	M	R	ET	+	-	+	7	1	0
7	79	M	R	ET	+	-	+	n/a	n/a	4
8	73	F	R	ET	+	-	-	8	1	0
9	88	F	L	ET	+	-	-	10	3	3
10	68	M	R	ET	+	-	+	12	3	4
11	76	M	R	ET	-	-	-	12	1	0
12	72	M	R	ET	-	-	-	9	2	0
13	78	M	R	ET	-	-	-	11	2	2
14	75	M	R	ET	+	+	-	12	4	3
15	88	M	R	ET	-	-	-	12	5	5
16	62	M	R	ET	+	n/a	-	12	3	n/a
17	80	M	R	ET	+	+	-	n/a	n/a	0
18	77	M	R	PD	+	-	-	10	2	1
19	87	F	R	ET	+	-	+	7	2	1
20	74	M	R	ET	+	-	-	12	4	3
21	68	M	R	ET	-	-	-	5	2	3
22	71	M	R	PD	-	-	-	5	0	1
23	79	F	R	PD	-	-	-	6	4	3
24	84	F	R	ET	+	+	+	9	3	10
25	72	M	L	ET	-	-	-	9	5	6
26	78	F	L	PD	-	-	-	11	7	5
27	75	F	R	ET	+	-	-	11	0	0
28	71	F	R	ET	-	-	-	8	3	4
29	74	M	R	ET	-	-	-	n/a	n/a	3
30	81	M	R	ET	-	-	-	n/a	n/a	1
Mean±SD	75.0±8.0							9.65±2.30	2.85±1.66	2.66±2.44

* Gait and balance disturbance

** Treated side; drawing score; evaluated in the MRgFUS operation room

*** Treated side; tremor + drawing scores; evaluated on the next day after MRgFUS

Abbreviations: FUS, focused ultrasound; FTM score, Fahn-Tolosa-Marín Clinical Rating Scale for Tremor score; SD, standard deviation; ET, essential tremor; PD, Parkinson's disease; n/a, not available.

Supplementary Table 3: Imaging features of patients with or without self-reported or physical exam-based side effect.

	MRI Features	Self-reported side effect		Physical exam-based side effect	
		Absence	*Presence*	*Absence*	*Presence*
FUS lesion volume	Volume of Zone A (ml)	0.26±0.11	0.32±0.12	0.29±0.11	0.30±0.14
	Volume of Zone B (ml)	**1.04±0.34**	**1.67±0.69**	1.31±0.56	1.80±0.81
	Fraction of Zone A / Zone B	**0.26±0.07**	**0.20±0.07**	0.24±0.08	0.18±0.05
Overlap between FUS lesions and THOMAS segmentations	Fraction of Zone A within VIM	**0.50±0.17**	**0.31±0.14**	0.43±0.18	0.27±0.12
	Fraction of Zone B within VIM	**0.23±0.07**	**0.14±0.07**	0.20±0.08	0.11±0.05
	Off Target Fraction of Zone A outside TH	**0.09±0.07**	**0.33±0.22**	0.19±0.19	0.37±0.23
	Off Target Fraction of Zone B outside TH	**0.27±0.08**	**0.52±0.13**	**0.38±0.15**	**0.57±0.14**
	Off Target Fraction of Zone A within TH	0.41±0.17	0.36±0.13	0.38±0.15	0.36±0.16
	Off Target Fraction of Zone B within TH	**0.50±0.10**	**0.34±0.09**	0.43±0.11	0.32±0.11
Distance between FUS core lesion and THOMAS segmentations	AP Distance of Centroid (VIM - Zone A) (mm)	1.66±1.08	1.82±1.04	1.70±1.05	1.95±1.05
	RL Distance of Centroid (VIM - Zone A) (mm)	0.82±0.72	0.79±1.25	0.63±0.77	1.36±1.66
	SI Distance of Centroid (VIM - Zone A) (mm)	**1.14±0.96**	**2.77±1.43**	1.90±1.40	2.82±1.63
	Absolute Distance of Centroid (VIM - Zone A) (mm)	**2.55±0.83**	**3.79±1.33**	3.01±1.17	4.20±1.35
Distance between FUS core lesion and standard coordinate	AP Distance of Centroid (Standard - Zone A) (mm)	0.52±0.87	0.31±0.82	**0.63±0.71**	**0.39±0.69**
	RL Distance of Centroid (Standard - Zone A) (mm)	1.12±1.07	0.62±0.82	0.76±0.91	0.94±1.08
	SI Distance of Centroid (Standard - Zone A) (mm)	0.55±0.89	0.23±1.14	0.40±1.08	0.21±0.99
	Absolute Distance of Centroid (Standard - Zone A) (mm)	1.99±0.57	1.67±0.50	1.81±0.52	1.72±0.64

Note: Fraction of Zone A (or B) within the VIM: volume of overlap between Zone A (or B) and VIM divided by the volume of Zone A (or B). Fraction of Zone A (or B) within the VIM: volume of overlap between Zone A (or B) and VIM divided by volume of Zone A (or B). Off Target Fraction of Zone A (or B) outside TH: volume of Zone A (or B) outside TH divided by volume of Zone A (or B). Off Target Fraction of Zone A (or B) within TH: volume of Zone A within TH but outside VIM divided by volume of Zone A (or B). Standard coordinate refers to the VIM target indirectly determined based on the AC-PC line.

The bolded items represent statistical tests with Benjamini–Hochberg corrected p-values < 0.05.

Abbreviations: FUS, focused ultrasound; THOMAS, THalamus Optimized Multi Atlas Segmentation; VIM, ventral intermediate; TH, thalamus; AP, anterior-posterior; RL, right-left, SI, superior-inferior.

Supplementary Table 4: Comparisons of imaging features between patients with and without side effect.

	MRI Features	Self-reported side effect		Physical exam-based side effect
		Gait/balance	Gait/balance > 1 month	Gait/balance
		z-statistics	*z-statistics*	*z-statistics*
FUS lesion volume	Volume of Zone A	-1.25	-1.01	-0.05
	Volume of Zone B	**-2.48**	-1.43	-1.47
	Fraction of Zone A / Zone B	**2.48**	0.70	2.06
Overlap between FUS lesions and THOMAS segmentations	Fraction of Zone A within VIM	**2.73**	1.69	2.16
	Fraction of Zone B within VIM	**3.24**	2.46	2.55
	Off Target Fraction of Zone A outside TH	**-3.54**	-2.31	-2.26
	Off Target Fraction of Zone B outside TH	**-4.47**	-2.67	**-2.94**
	Off Target Fraction of Zone A within TH	0.57	1.22	0.00
	Off Target Fraction of Zone B within TH	**3.37**	1.84	1.96
Distance between FUS core lesion and THOMAS segmentations	AP Distance of Centroid (VIM - Zone A)	0.57	-0.75	0.64
	RL Distance of Centroid (VIM - Zone A)	0.70	-0.65	-0.88
	SI Distance of Centroid (VIM - Zone A)	**3.07**	1.12	1.67
	Absolute Distance of Centroid (VIM - Zone A)	**-2.73**	-1.32	-2.01
Distance between FUS core lesion and standard coordinate	AP Distance of Centroid (Standard - Zone A)	0.47	-1.00	**2.83**
	RL Distance of Centroid (Standard - Zone A)	1.37	0.08	-0.33
	SI Distance of Centroid (Standard - Zone A)	0.79	0.40	0.38
	Absolute Distance of Centroid (Standard - Zone A)	1.19	-0.46	0.38

Note: Abbreviations: FUS, focused ultrasound; THOMAS, THalamus Optimized Multi Atlas Segmentation; VIM, ventral intermediate; TH, thalamus; AP, anterior-posterior; RL, right-left, SI, superior-inferior.

Supplementary Table 5: Correlation coefficients and *p*-values between imaging features and post-FUS FTM scores.

	MRI Features	Correlation with post-FUS FTM	
		Coefficient r	*p-value*
FUS lesion volume	Volume of Zone A	-0.15	0.44
	Volume of Zone B	0.03	0.87
	Fraction of Zone A / Zone B	-0.25	0.20
Overlap between FUS lesions and THOMAS segmentations	Fraction of Zone A within VIM	0.07	0.73
	Fraction of Zone B within VIM	-0.18	0.33
	Off Target Fraction of Zone A outside TH	-0.21	0.28
	Off Target Fraction of Zone B outside TH	-0.12	0.54
	Off Target Fraction of Zone A within TH	0.29	0.13
	Off Target Fraction of Zone B within TH	0.42	< 0.05
Distance between FUS core lesion and THOMAS segmentations	AP Distance of Centroid (VIM - Zone A)	0.02	0.92
	RL Distance of Centroid (VIM - Zone A)	0.30	0.12
	SI Distance of Centroid (VIM - Zone A)	0.40	< 0.05
	Absolute Distance of Centroid (VIM - Zone A)	-0.13	0.52
Distance between FUS core lesion and standard coordinate	AP Distance of Centroid (Standard - Zone A)	-0.04	0.84
	RL Distance of Centroid (Standard - Zone A)	0.34	0.06
	SI Distance of Centroid (Standard - Zone A)	0.05	0.82
	Absolute Distance of Centroid (Standard - Zone A)	0.09	0.65

Note: *P*-values in the table represent uncorrected *p*-values.

Abbreviations: FUS, focused ultrasound; FTM score, Fahn-Tolosa-Marín Clinical Rating Scale for Tremor score; THOMAS, THalamus Optimized Multi Atlas Segmentation; VIM, ventral intermediate; TH, thalamus; AP, anterior-posterior; RL, right-left, SI, superior-inferior.

Supplementary Table 6: Correlation coefficients and *p*-values between imaging features and reduction in drawing scores after MRgFUS.

	MRI Features	Correlation with score reduction	
		Coefficient r	*p-value*
FUS lesion volume	Volume of Zone A	0.06	0.77
	Volume of Zone B	0.22	0.28
	Fraction of Zone A / Zone B	-0.25	0.21
Overlap between FUS lesions and THOMAS segmentations	Fraction of Zone A within VIM	-0.25	0.22
	Fraction of Zone B within VIM	-0.30	0.14
	Off Target Fraction of Zone A outside TH	0.38	0.06
	Off Target Fraction of Zone B outside TH	0.36	0.07
	Off Target Fraction of Zone A within TH	0.03	0.88
	Off Target Fraction of Zone B within TH	-0.28	0.17
Distance between FUS core lesion and THOMAS segmentations	AP Distance of Centroid (VIM - Zone A)	-0.11	0.58
	RL Distance of Centroid (VIM - Zone A)	-0.21	0.30
	SI Distance of Centroid (VIM - Zone A)	-0.43	< 0.05
	Absolute Distance of Centroid (VIM - Zone A)	0.26	0.20
Distance between FUS core lesion and standard coordinate	AP Distance of Centroid (Standard - Zone A)	-0.20	0.33
	RL Distance of Centroid (Standard - Zone A)	-0.01	0.96
	SI Distance of Centroid (Standard - Zone A)	-0.16	0.43
	Absolute Distance of Centroid (Standard - Zone A)	-0.36	0.08

Note: *P*-values in the table represent uncorrected *p*-values.

Abbreviations: FUS, focused ultrasound; FTM score, Fahn-Tolosa-Marín Clinical Rating Scale for Tremor score; THOMAS, THalamus Optimized Multi Atlas Segmentation; VIM, ventral intermediate; TH, thalamus; AP, anterior-posterior; RL, right-left, SI, superior-inferior.

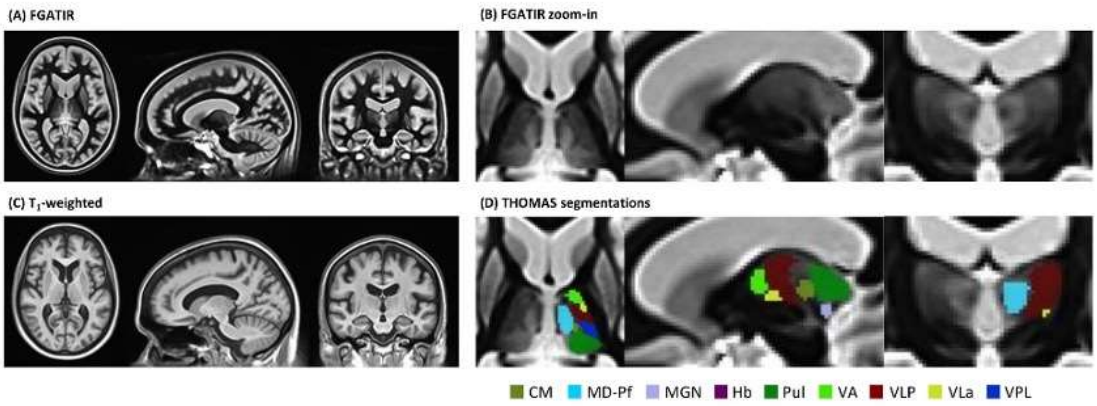

Supplementary FIG 1. The cohort template FGATIR image (A: whole brain; B: zoom-in), T_1-weighted image (C) and corresponding THOMAS segmentations (D). FGATIR, Fast Gray Matter Acquisition T1 Inversion Recovery; THOMAS, THalamus Optimized Multi Atlas Segmentation; VA, ventral anterior nucleus; VLa, ventral lateral anterior nucleus; VLP, ventral lateral posterior nucleus; VPL, ventral posterior lateral nucleus; Pul, pulvinar nucleus; CM, centromedian nucleus; MD-Pf, mediodorsal-parafascicular nucleus; MGN, medial geniculate nucleus.

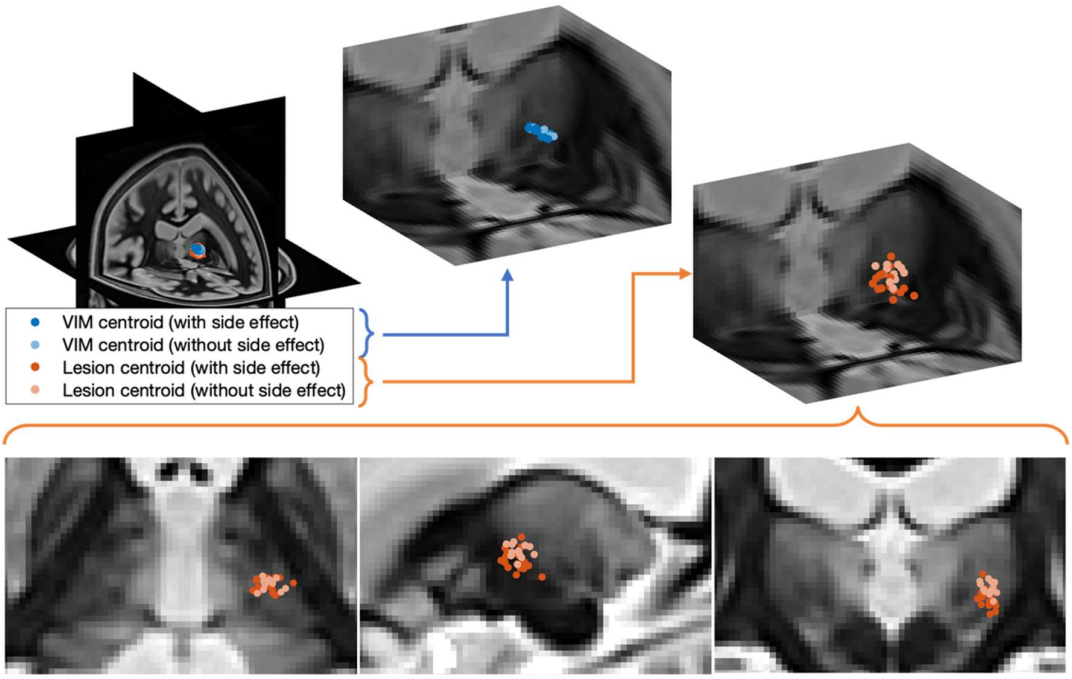

Supplementary FIG 2. Plots of VIM and lesion centroids for patients with and without side effects are depicted in the population-specific template space. Visually, the centroid of lesions in patients with side effects appears to be positioned more inferior compared to those without side effects. VIM, ventral intermediate nucleus.

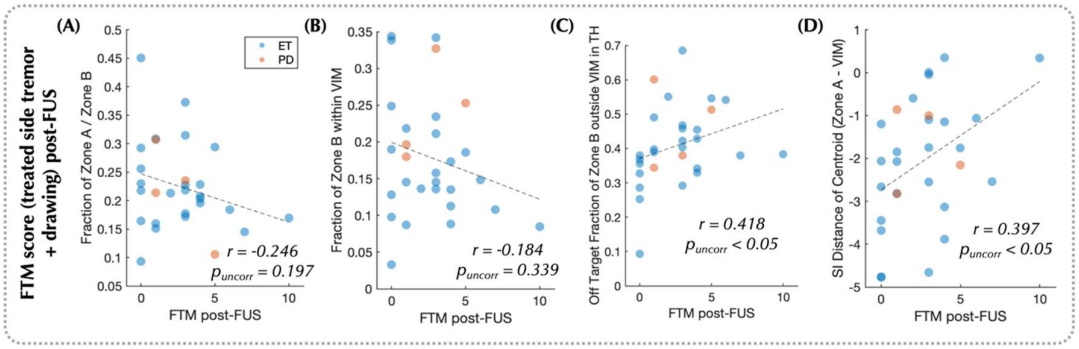

Supplementary FIG 3. Correlation between imaging features and post-FUS FTM scores. Although no significant correlations between imaging features and FTM scores were found after Benjamini–Hochberg multiple statistics correction, moderate positive correlations were observed between the VIM – Zone A centroid SI distance and FTM scores (D). Zone A volume and the fraction of Zone A within VIM were found to have weak or no correlation with the clinical tremor assessments (A and B). FTM score, Fahn-Tolosa-Marín Clinical Rating Scale for Tremor score; FUS, focused ultrasound; ET, essential tremor; PD; Parkinson's disease; VIM, ventral intermediate; TH, thalamus; SI, superior-inferior.